SCIENCE CHINA
Earth Sciences

• RESEARCH PAPER •

July 2013 Vol.56 No.7: 1254–1265
doi: 10.1007/s11430-012-4443-y

Two interannual variability modes of the Northwestern Pacific Subtropical Anticyclone in boreal summer

HE Chao[1,2], ZHOU TianJun[1*], ZOU LiWei[1] & ZHANG LiXia[1]

[1] *The State Key Laboratory of Numerical Modeling for Atmospheric Sciences and Geophysical Fluid Dynamics (LASG), Institute of Atmospheric Physics, Chinese Academy of Sciences, Beijing 100029, China;*
[2] *Graduate University of Chinese Academy of Sciences, Beijing 100049, China*

Received January 4, 2012; accepted March 30, 2012; published online July 18, 2012

Using the reanalysis data and 20th century simulation of coupled model FGOALS_gl developed by LASG/IAP, we identified two distinct interannual modes of Northwestern Pacific Subtropical Anticyclone (NWPAC) by performing Empirical Orthogonal Function (EOF) analysis on 850 hPa wind field over the northwestern Pacific in summer. Based on the associated anomalous equatorial zonal wind, these two modes are termed as "Equatorial Easterly related Mode" (EEM) and "Equatorial Westerly related Mode" (EWM), respectively. The formation mechanisms of these two modes are similar, whereas the maintenance mechanisms, dominant periods, and the relationships with ENSO are different. The EEM is associated with El Niño decaying phase, with the anomalous anticyclone established in the preceding winter and persisted into summer through local positive air-sea feedback. By enhancing equatorial upwelling of subsurface cold water, EEM favors the transition of ENSO from El Niño to La Niña. The EWM is accompanied by the El Niño events with long persistence, with the anomalous anticyclone formed in spring and strengthened in summer due to the warm Sea Surface Temperature anomalies (SSTA) forcing from the equatorial central-eastern Pacific. The model well reproduces the spatial patterns of these two modes, but fails to simulate the percentage variance accounted for by the two modes. In the NCEP reanalysis (model result), EEM (EWM) appears as the first mode, which accounts for 35.6% (68.2%) of the total variance.

Northwestern Pacific Subtropical Anticyclone, interannual variability mode, equatorial easterly related mode, equatorial westerly related mode, ENSO

Citation: He C, Zhou T J, Zou L W, et al. Two interannual variability modes of the Northwestern Pacific Subtropical Anticyclone in boreal summer. Science China: Earth Sciences, 2013, 56: 1254–1265, doi: 10.1007/s11430-012-4443-y

The Northwestern Pacific Subtropical High or Northwestern Pacific Subtropical Anticyclone (NWPSH or NWPAC) is a key component of the East Asia-Western Pacific monsoon system. The intensity and position of the NWPAC are closely associated with East Asian summer monsoon rainfall on various timescales. On synoptic timescale, the East Asian summer rain belt is located on the western flank of the NWPAC and is influenced by the oscillation of the NWPAC. On intraseasonal time scale in summer, the abrupt northward jumps of its ridge leads to the establishment of rainy season over South China, the Yangtze-Huai River, and North China [1]. Interannual NWPAC anomalies are associated with interannual variation of water vapor transport and typical rainfall patterns in China [2, 3]. The NWPAC is an important bridge that connects El Niño-South Oscillation (ENSO) with East Asian climate [4]. Investigation on the variation of the NWPAC helps us understand the mechanisms of monsoon variability and is beneficial to the improvement of the short term climate prediction.

The subtropical North Pacific is dominated by the NWPAC in boreal summer. The NWPAC is centered over the eastern (central-western) Pacific at 850 hPa (500 hPa)

*Corresponding author (email: zhoutj@lasg.iap.ac.cn)

[5]. The global land-sea distribution determines the atmospheric heating climatology in boreal summer subtropics, which is characterized by long-wave cooling in eastern oceans, sensible heating in western continents, and latent heating in eastern continents. The specific heating profiles induce typical wind field and thus determine the subtropical circulation climatology [6, 7]. However, the region with the strongest interannual variability is not located at the center of the NWPAC, but on its western edge [8–10]. Moreover, the western edge of the NWPAC has the strongest interannual variability all over the subtropical northern hemisphere in summer [11]. Therefore, attention should be paid to the western portion of the NWPAC when we study the variability, while paid to its center when we study the climatology.

The characteristics and mechanisms for the interannual variability of the NWPAC have been well documented in previous researches. The East Asian summer monsoon gets strengthened and Meiyu front gets suppressed when the NWPAC extends northward, and vice versa [3]. The meridional displacement of the NWPAC has a close relationship with its zonal displacement. A northward shift of the NWPAC is generally accompanied with an eastward displacement, whereas a southward shift is generally accompanied with a westward displacement. When the eastern part of the NWPAC tilts southward, the western part usually tilts northward [12]. The first Empirical Orthogonal Function (EOF) mode of 850 hPa zonal wind over the northwestern Pacific (NWP) is a "tropical mode", which is affected by tropical SST and highly predictable. The second mode is a "meridional mode", which is dominated by atmospheric internal processes and poorly predictable [13].

The interannual variability of the NWPAC is closely related to tropical SSTA. Take El Niño decay year for example. Wang et al. [14] documented that air-sea interaction over the tropical Pacific Ocean (especially NWP) plays a key role in maintaining the anomalous NWPAC from boreal winter to early summer, while Indian Ocean plays a minor role. Xie et al. [15] argued the Indian Ocean acts as the bridge connecting ENSO in winter and the NWPAC in the subsequent summer. Warm SSTA over the Indian Ocean is usually forced by ENSO and forces an anomalous anticyclone over the NWP through Kelvin wave and wave-induced Ekman divergence in boreal summer. Wu et al. [16, 17] showed that the anomalous summer NWPAC is attributed to the combined effects of local SSTA over the NWP and remote SSTA over the tropical Indian Ocean (TIO). The local cold SSTA is dominant in June, whereas TIO SSTA is dominant in July and August. Some studies suggested that the NWPAC is able to affect the development and phase transition of ENSO. Equatorial upwelling is enhanced by the anomalous easterly on the southern flank of the anomalous NWPAC, favoring the transition from El Niño into La Niña [18, 19].

Recent studies found that the interannual variability of the NWPAC exhibits different characters. The NWPAC index based on 500 hPa geopotential height is featured by two interannual periods, i.e. 2–3 years and 3–5 years. The 2–3 year oscillation is equivalent barotropic and closely related to maritime continent convection, whereas the 3–5 year oscillation is baroclinic and connected with negative atmospheric heat source associated with local cold SSTA [9, 10]. Although the first two EOF modes of 850 hPa wind over the NWP are both characterized by an anomalous NWPAC, their mechanisms differ. The first mode appears in the summer when ENSO transits from El Niño to La Niña, whereas the second mode is seen in the El Niño persisting summer [20]. However, the previous work mainly focuses on decadal change, and the mechanism of the interannual variability remains unknown. This study aims to answer the following questions: what are the dominant modes of interannual variability of the NWPAC represented by 850 hPa wind field? How do they emerge, maintain, and interact with tropical oceans?

The variability of the NWPAC involves air-sea interactions over the Indo-Pacific region. Ocean-atmosphere coupled models are useful tools in understanding the variability of the NWPAC and the underlying air-sea interactions. Less attention has been paid to assessing the ability of coupled models in simulating the NWPAC, especially its interannual variability. The Flexible Global Ocean-Atmosphere-Land-Sea ice model (FGOALS) [21, 22] developed by IAP/LASG has been widely used in climate simulation studies [23–26]. How well can FGOALS capture the interannual modes of the NWPAC? This is another issue that will be addressed in the study. Since the NWPAC has a close relationship with the East Asian summer monsoon, this work is of great importance for understanding the mechanisms and predicting /projecting the future change of the East Asian monsoon using coupled models.

1 Data, model and methods

The following datasets are used: (1) National Center for Environmental Prediction/ National Center for Atmospheric Research (NCEP/NCAR) atmospheric reanalysis data from 1950 to 1999, with a 2.5°×2.5° horizontal resolution [27]; (2) Extend Reconstructed Sea Surface Temperature version 2 (ERSST v.2) by NOAA from 1950 to 1999, with a 2°×2° horizontal resolution [28].

The output of the 20th century coupled model simulation (20C3M) experiment of FGOALS_gl model is employed. FGOALS_gl is a fast version climate system model. The four component models, viz. atmospheric model, oceanic model, land surface model, and sea ice model, are coupled together through the NCAR CCSM2 coupler. The atmosphere component is a low resolution version of Grid Atmospheric Model of IAP/LASG (GAMIL), with a horizontal resolution of 5°(longitude)×4°(latitude), and 26 vertical levels in a σ-p coordinates. The ocean component is LASG/

IAP Climate System Ocean Model (LICOM), with a horizontal resolution of 1°×1° and 30 vertical levels (12 levels at the top 300 m). The land and sea-ice components are NCAR CLM and CSIM, respectively. Details about FGOALS_gl are described in Zhou et al. [29].

The 20C3M simulation is forced by historical atmospheric radiative forcing field provided by IPCC AR4, which consists of natural forcing (solar activity, volcanic aerosols) and anthropogenic forcing (greenhouse gas emissions and sulfate aerosols) [30]. The simulation period covers 1860 to 2000 [31]. The period 1950–1999 is selected for comparison with the reanalysis data.

Traditional definitions of the NWPAC are usually based on 5880gpm contour at 500 hPa. Recent studies show that the NWPAC is more evident at the lower troposphere [13, 20, 32, 33]. Compared with the middle and upper troposphere, the lower troposphere wind field better represents water vapor transport associated with precipitation [5]. Therefore, wind at 850 hPa is selected to investigate the interannual variability of the NWPAC in this study. It is unreasonable to compare the NWPAC between model and reanalysis using a fixed contour with original geopotential height [34], since the average geopotential height in the coupled model differs from that in the reanalysis data. For instance, if the zonal mean 500 hPa geopotential height derived from the model is higher than the reanalysis, it would be erroneously concluded by a "wider and stronger" NWPAC in the simulation based on 5880 gpm contour at 500 hPa. To overcome this problem, we subtract the zonal belt mean value between equator and 45°N from the geopotential height field, and use the departure field to represent the position of NWPAC. This method has also been adopted by some previous works [6, 34].

Many indices are available to study the variation of the NWPAC [5, 35], such as area index, intensity index, ridgeline index, northern edge index, and western ridge point index defined by Chinese Meteorological Administration using 500 hPa geopotential height field [36]. However, these indices are not convenient for reanalysis data and model simulation [35]. The NWPAC index employed in this work is defined as the difference of 850 hPa zonal wind between a north region (20°–30°N, 110°–140°E) and a south region (5°–15°N, 100°–130°E) [32].

To reveal the dominant interannual variability modes, multivariable EOF analysis [37] is applied to 850 hPa wind field over the northwestern Pacific (100°–170°W, 0°–40°N). Anomalous SST and 850 hPa wind field are regressed onto the PC time series to discuss the mechanism of the NWPAC. As in Park et al. [20], normalization is not applied before EOF analysis in order to retain the strength of original vector component. Eight years high pass Fourier filter is applied before doing EOF analysis since we only focus on the interannual variation.

2 Climatology of summer NWPAC

The climatological summer NWPAC for 1950–1999 is shown in Figure 1. In NCEP data, the NWPAC at the lower troposphere (below 700 hPa) centers at the eastern Pacific (35°E, 150°W) and extends to the NWP. The ridge line of the NWPAC exhibits a northeast-southwest direction (Figure 1(a)–(c)). The northeastern and southwestern parts of the ridge line is seen at 30°N, 180°E/W and 20°N, 130°E, respectively. The 500 hPa NWPAC shifts to the west of that in the lower troposphere, centered at 25°N, 160°E (Figure 1(d)). The intensity of the NWPAC decreases with height (Figure 1(a)–(d)), almost vanishing at 300 hPa (figure not shown). The NWPAC at 850 hPa is obviously stronger than that at 500 hPa in terms of the density of contours and the strength of anticyclonic wind field.

The simulated zonal mean geopotential height on each isobaric surface is higher than that in the NCEP reanalysis data. After subtracting the zonal mean geopotential height, the model has a good performance in reproducing the lower troposphere NWPAC, but with the center being southward shifted (Figure 1(e)–(g), shading). The simulated NWPAC at 500 hPa is stronger than the NCEP reanalysis data, and the center shifts eastward by about 10° (Figure 1(h), shading). Generally, FGOALS_gl can reasonably reproduce the climatology of the NWPAC, with a higher simulation skill at 850 hPa than 500 hPa. Therefore, FGOALS_gl can be used to analyze the interannual variability of the NWPAC.

3 Dominant modes of interannual variability

The NWPAC index and the corresponding power spectra are shown in Figure 2. Two peaks of the NWPAC power spectra are evident in both the NCEP reanalysis and the simulation. One peak is 2–3 years (quasi-two years) and the other one is quasi-five years.

The first two EOF modes and the corresponding PC time series of summer NWP wind at 850 hPa derived from the NCEP reanalysis data are shown in Figure 3. The first two EOF modes are both featured by an anticyclonic circulation to the northeast of the Philippines, which coincide with the climatological summer NWPAC at 850 hPa (Figure 1(b)), indicating an enhancement of the NWPAC. The most striking difference of the first two modes is the wind along the equator. EOF1 is associated with anomalous equatorial easterly, whereas EOF2 shows anomalous westerly. In addition, the center of the anomalous anticyclone in EOF1 shifts southward in comparison to that of EOF2. The EOF1 derived from the NCEP reanalysis in this study is highly consistent with that derived from NCEP2 reanalysis by Park et al. [20]. However, the EOF2 based on NCEP2 shows an eastward shifted NWPAC and has a cyclonic circulation around 10°N, 150°E. The first mode and the second mode

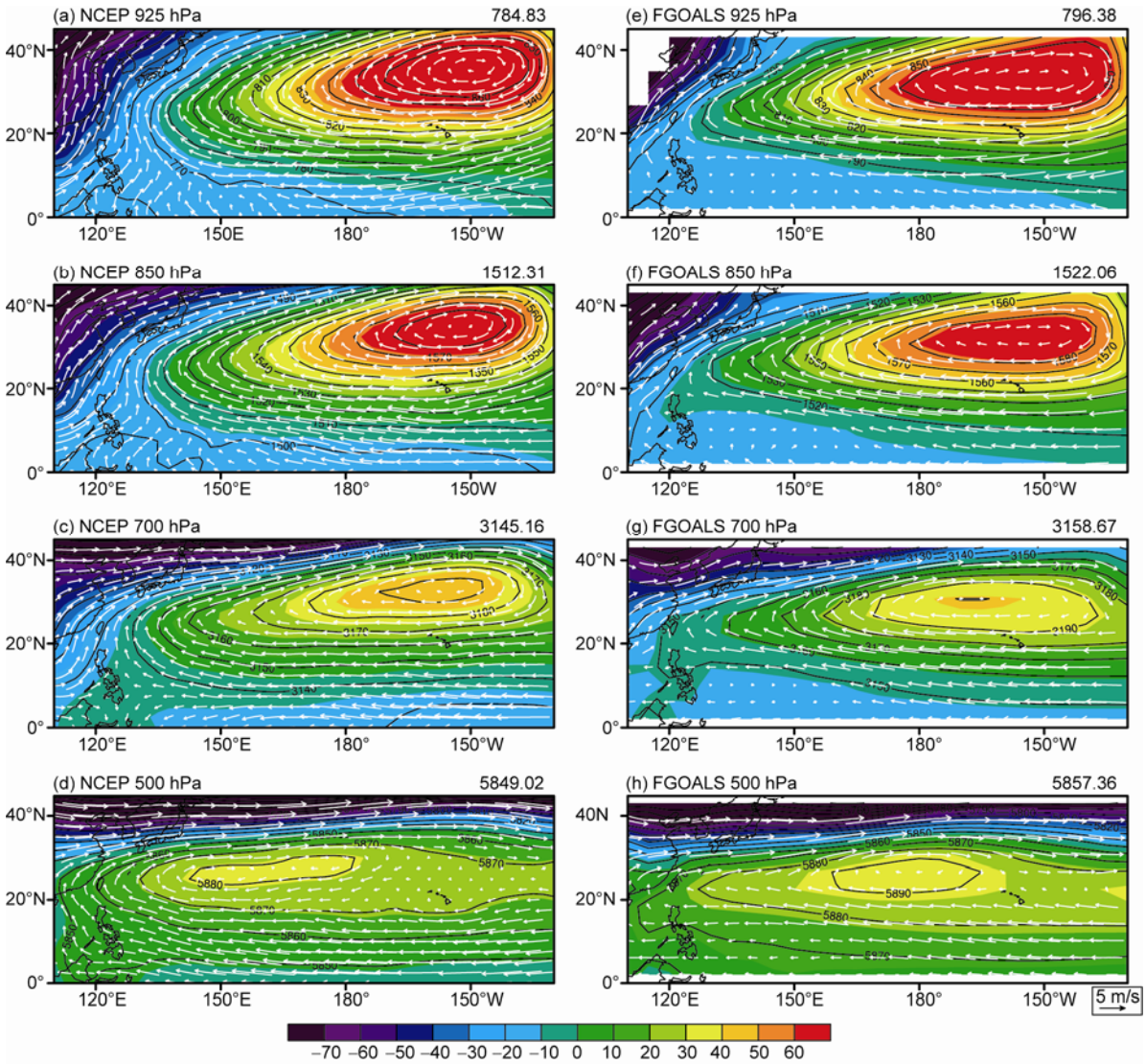

Figure 1 Summer (JJA) climatological geopotential height field (black contour) and its departure from zonal mean (shading), with wind field (white arrow) for ((a), (e)) 925 hPa, ((b), (f)) 850 hPa, ((c), (g)) 700 hPa, ((d), (h)) 500 hPa. (a)–(d) are for NCEP reanalysis and (e)–(h) are for model result. Zonal mean geopotential height of 0°–45°N is marked on the upper-right corner of each panel.

are dominated by quasi-two year and quasi-five year oscillation, respectively (Figure 3(c), (f)).

The first two EOF modes and the corresponding PC time series derived from FGOALS_gl are shown in Figure 4. The anomalous anticyclonic circulation to the northeast of the Philippines is well captured in the simulation. The anomalous equatorial zonal winds associated with the two modes are also opposite to each other. However, the simulated anomalous anticyclone shifts eastward in comparison to that in NCEP reanalysis. The simulated EOF2 (EOF1) corresponds to EOF1 (EOF2) in the NCEP reanalysis data, and both exhibit anomalous easterly (westerly) along the equator. The power spectra of simulated PC2 (PC1) time series shows dominating quasi-two year (quasi-five years) oscillation (Figure 4(c), (f)), consistent with PC1 (PC2) in reanalysis data.

The consistency between NCEP reanalysis data and FGOALS_gl suggests there are two distinct interannual variability modes of the NWPAC, featuring distinct equatorial zonal wind and dominant oscillating period. These two modes are termed as "Equatorial Easterly related Mode" (EEM) and "Equatorial Westerly related Mode" (EWM) in terms of equatorial zonal wind direction, respectively.

The simulated EWM accounts for 68.2% of the total variance, which is much higher than the reanalysis. This model deficiency is probably due to the simulated ENSO phase and period. The simulated ENSO generally peaks in spring-summer but not in winter as in observations [24]. It will result in stronger ENSO signal in summer and exert excessively strong influence on the summer NWPAC. Since the ENSO period in the model is dominated by quasi-five years [24], this could explain why the simulated NWPAC

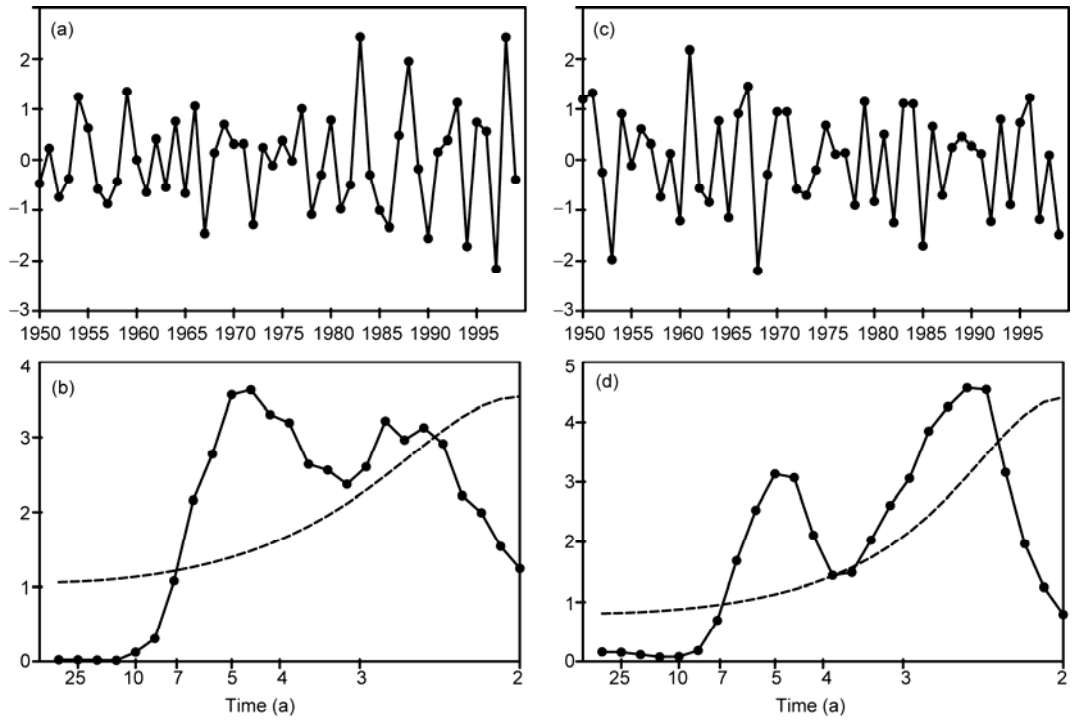

Figure 2 (a) Time series of NWPAC intensity index derived from NCEP reanalysis, and (b) the corresponding power spectra of NWPAC index (solid line) with the power spectra of Markov red noise (dashed line). (c)–(d) are the same as in (a)–(b) but for model result.

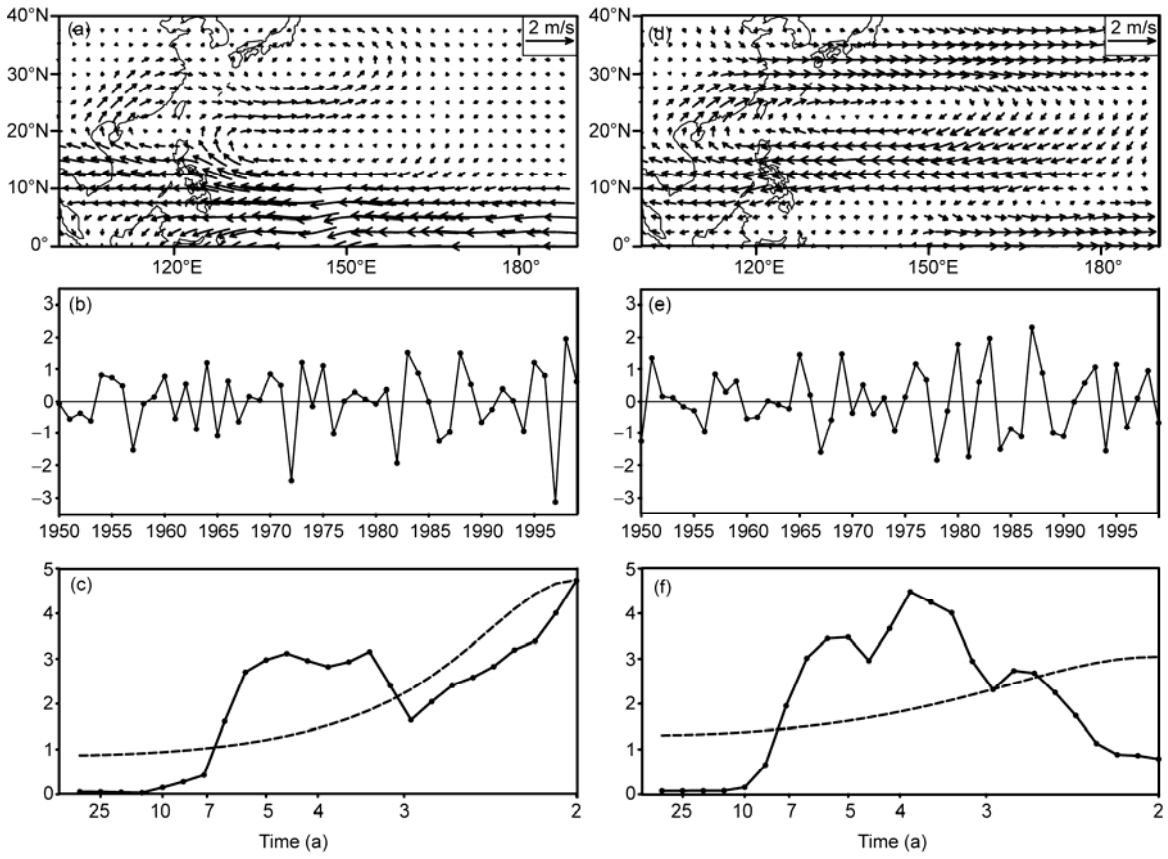

Figure 3 The first two modes obtained by multivariate EOF analysis on the summer 850 hPa wind over the northwestern Pacific Ocean derived from NCEP reanalysis data. (a), (d) the spatial pattern, (b), (e) PC time series, (c), (f) the power spectra of the PC (solid line) and Markov red noise (dashed line). (a)–(c) are for the first mode whereas (d)–(f) are for the second mode. The percentages of variance explained by the first and the second mode are 35.6% and 19.3%, respectively.

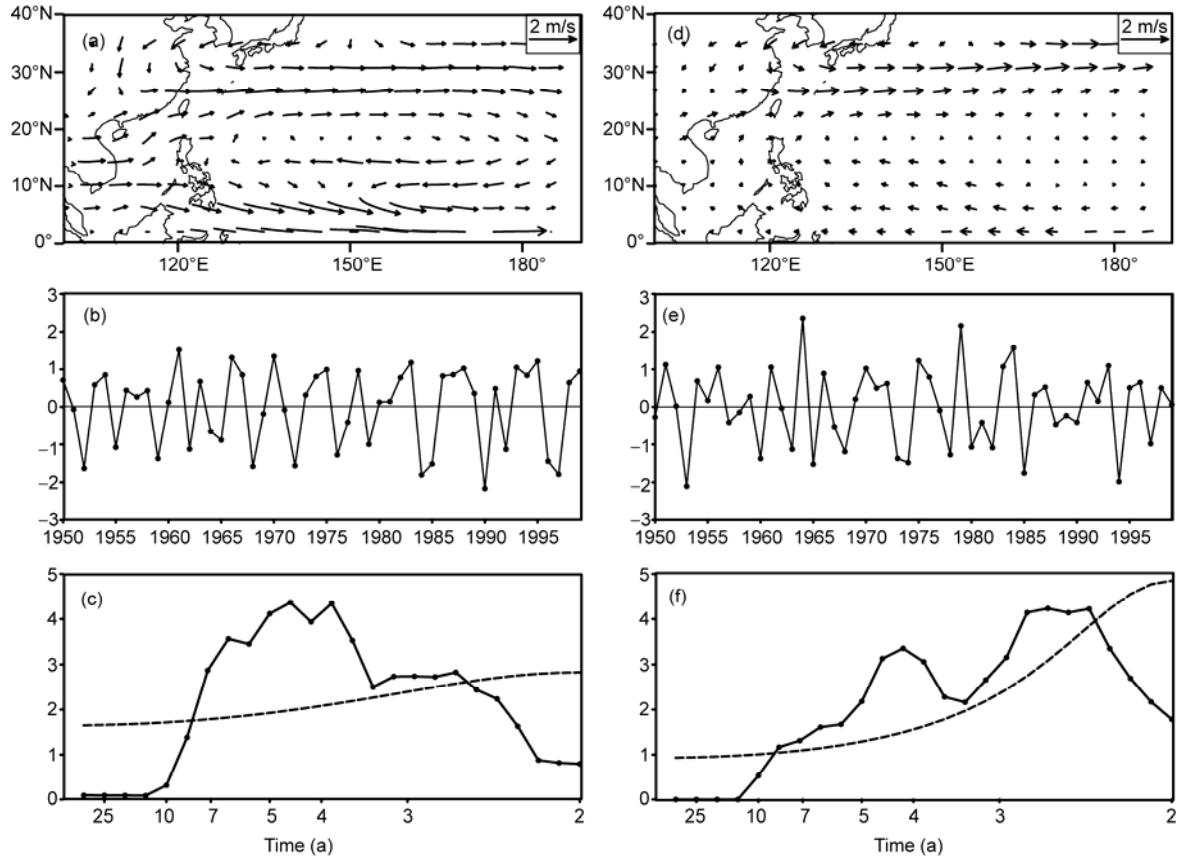

Figure 4 Same as in Figure 3, but for model result. The percentages of variance explained by the first and the second mode are 68.2% and 10.7%, respectively.

has a stronger quasi-five year period and why EWM accounts for too large a portion of variance. By performing EOF analysis on the simulated 850 hPa wind field in all seasons, it is found that EOF1 in summer explains the largest percentages of variance compared with other seasons, supporting the above hypothesis.

4 Mechanisms for interannual variability modes

To understand the related mechanism for the interannual variation of the summer NWPAC, the associated SSTA and circulation anomalies over the Indo-Pacific from the preceding fall to concurrent summer are shown in Figure 5 by regressing the SSTA and wind onto the first two PCs of NCEP data (Figure 3(b), (e)).

The evolution of SSTA shows that the EEM in the reanalysis corresponds to El Niño decay and transition to La Niña (Figure 5(a)–(d)). The anomalous NWPAC emerges in the preceding winter, which appears as a large-scale subtropical anticyclonic circulation from 120°E to 150°W. This large-scale anticyclonic circulation has two anticyclone centers, consistent with the two trigger mechanisms proposed by Wang et al. [14]. One of them is located at the western Pacific (15°N, 140°E) and may be associated with cold surge. The other is centered at the central Pacific (25°N at date line) and may be resulted from the eastern Pacific warm SSTA forcing.

The anomalous NWPAC in EEM is maintained from winter to subsequent spring and summer by local air-sea interaction, as suggested by Wang et al. [14]. Under the northeasterly trade background in winter-half year, the anomalous northeasterly on the eastern flank of the anomalous anticyclone amplifies the wind speed, cooling the local SST by enhancing evaporation. The cooled SST triggers anticyclonic Rossby wave to its west [38], which in turn enhances the anomalous northeasterly. Similarly, anomalous southwesterly on the western flank of anomalous anticyclone reduces the wind speed, warming the SST and enhancing the anomalous southwesterly. This positive air-sea feedback maintains the anomalous NWPAC during El Niño decaying phase, as seen in Figure 5(b)–(d). From spring to summer, the intensity of the anomalous NWPAC has weakened (Figure 5(c)–(d)), possibly due to the reversal of background climatological wind after the NWP summer monsoon's onset. This further confirms the key role of local air-sea feedback in the maintenance of the anomalous NWPAC.

EWM in NCEP is related to El Niño that persists from the preceding fall to concurrent summer (Figure 5(e)–(h)).

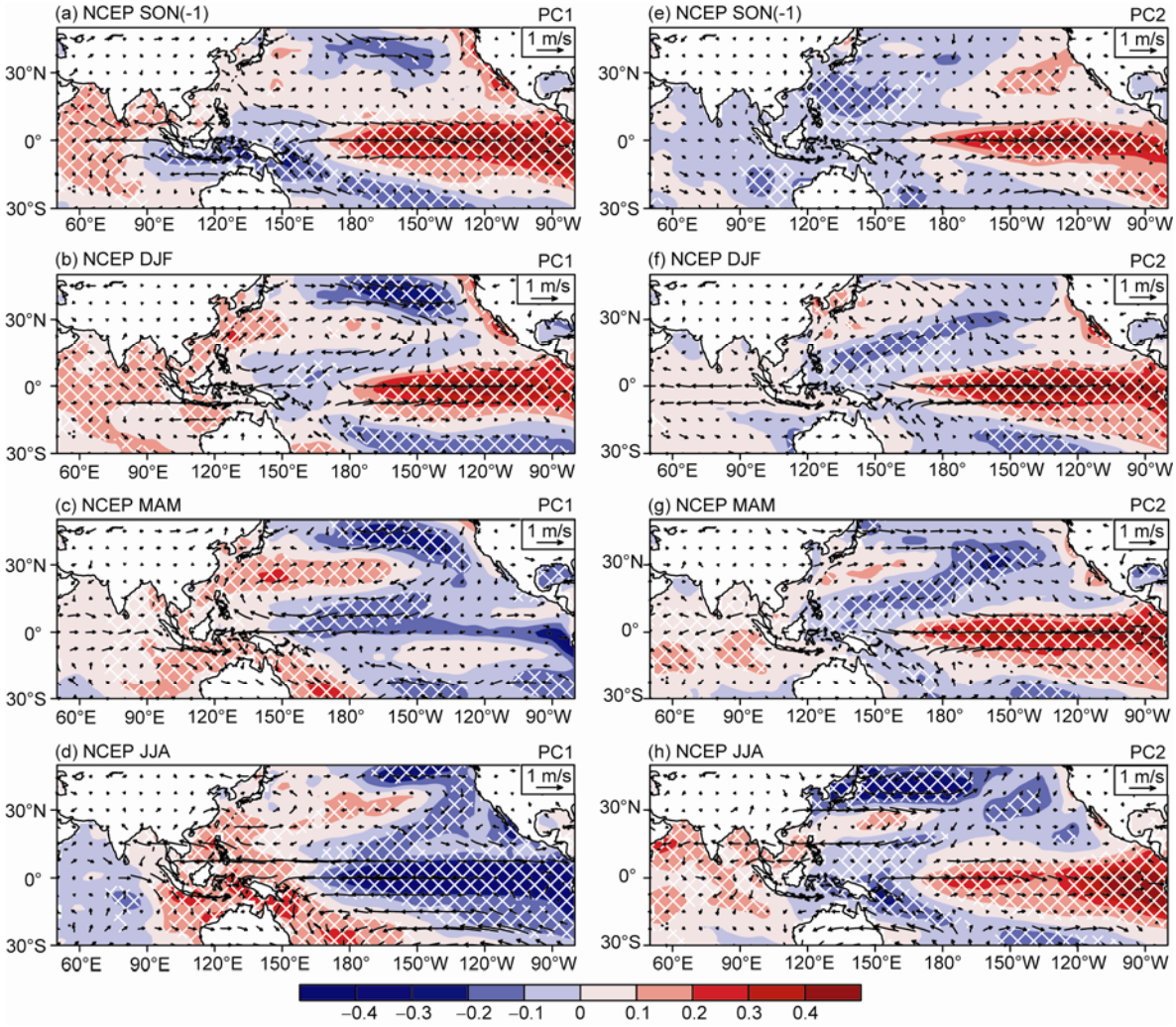

Figure 5 (a)–(d) SSTA (shaded) and 850 hPa wind (arrow) in the previous fall, winter, spring and concurrent summer regressed onto PC1 derived from NCEP data. (e)–(h) are the same as (a)–(d) except for PC2. Regions exceeding 95% confidence level are shown as white cross in each panel.

The anomalous NWPAC emerges in spring (anomalous anticyclone to the east of Japan is also evident in the previous winter, but it should be taken as mid-latitude anticyclone rather than "subtropical anticyclone" because its center is located to the north of 30°N). The anomalous NWPAC gets strengthened from spring to summer, indicating it may not be a persistent signal from the previous season but is forced by the simultaneous warm SSTA over the eastern Pacific.

How does equatorial eastern Pacific warm SSTA contribute to the formation of the anomalous NWPAC? Eastern Pacific warming induces a cyclonic circulation near the dateline as Rossby wave response (Figure 5(f)). Anomalous northeasterly on its western flank induces cold SSTA to develop over the central Pacific. As Rossby wave responses to the negative heat source in the central Pacific associated with cold SSTA, anomalous anticyclone forms over the NWP in spring (Figure 5(g)). The anomalous NWPAC gets further strengthened in summer (Figure 5(h)). In fact, the formation mechanism of the anomalous NWPAC in EWM is similar as in EEM (Figure 5(b)), although their maintenance mechanism and associated ENSO phase are different.

The simulated SSTA and wind anomalies at 850 hPa regressed onto model PCs are shown in Figure 6. The results of simulation resemble those of the reanalysis. The simulated EWM is accompanied by El Niño persisting from the preceding fall, with the anomalous NWPAC emerging in spring (Figure 6(a)–(d)). In FGOALS_gl, the warm SSTA over the central-eastern Pacific extends excessively westward (reaching the coast of maritime continent), with a stronger equatorial easterly anomaly than in reanalysis.

The corresponding mechanism for the anomalous NWPAC in FGOALS_gl is nearly the same as that in the NCEP data. An anomalous cyclonic circulation emerges around 5°–10°N at dateline in spring and summer (Figure 6(c)–(d)). On the northern flank of this cyclonic circulation, there exists an east-west tilted cold SSTA, dominated by anomalous easterly. The anomalous NWPAC is composed

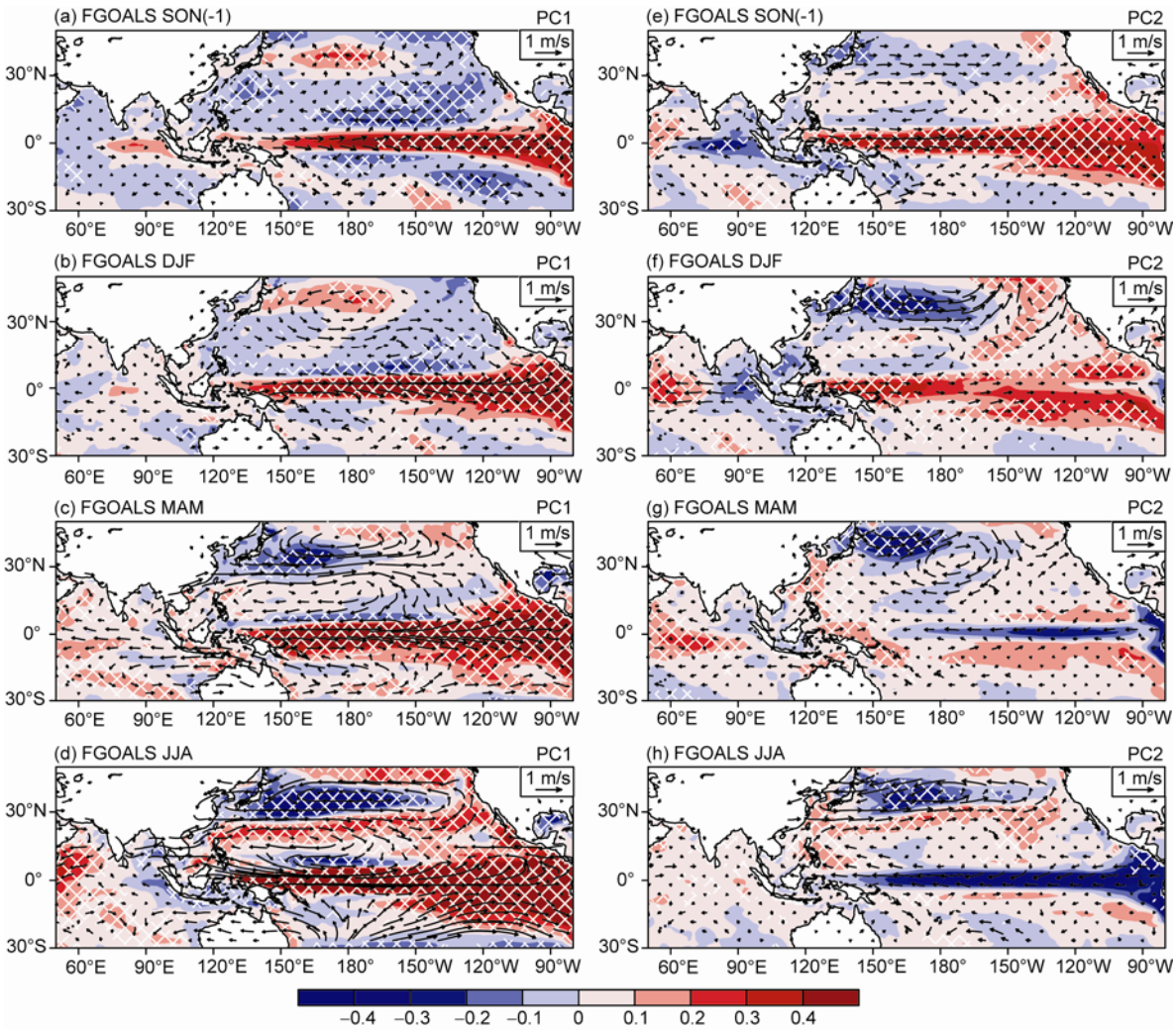

Figure 6 Same as in Figure 5, but for model result.

of this anomalous easterly and an anomalous westerly to its north. Different from the northeast-southwest tilting pattern of subtropical SSTA belts in NCEP data, the simulated east-west tilting pattern is possibly due to the excessively strong zonal wind anomalies in the model.

The simulated EEM is associated with El Niño decaying phase in the preceding fall and winter. Different from the reanalysis, the La Niña-like cold SSTA in the equatorial central-eastern Pacific in spring and summer is not statistically significant (Figure 6(g), (h)). The anomalous NWPAC has formed since the preceding fall (Figure 6(e)). A northeast-southwest tilting cold (warm) SSTA belt exists and sustains over the subtropical central (western) Pacific (Figure 6(f)–(h)), associated with anomalous northeasterly (southwesterly), indicating the role of local air-sea interaction. The simulated EEM is not accompanied by a La Niña development, implying that the anomalous NWPAC of simulated EEM cannot efficiently drive the phase transition from El Niño to La Niña. This deficiency leads to a much weaker quasi-two year oscillation in the ENSO-monsoon system and smaller percentage variance explained by the EEM in the model.

The anomalous NWPAC plays an interactive role in ENSO phase transition. Anomalous easterly on the southern flank of the anomalous NWPAC leads to anomalous equatorial oceanic upwelling, which cools the SST over the equatorial central Pacific, and favors La Niña formation in the subsequent fall and winter. This mechanism accounts for the quasi-two year oscillation of the ENSO and NWPAC. However, whether this mechanism works depends on whether the anomalous NWPAC is closely located to the equator [18]. In the NCEP data, the anomalous NWPAC of EEM is closer to the equator than that of EWM (Figure 3(a), (d)), so the anomalous NWPAC in EEM is able to efficiently influence the evolution of ENSO.

To verify the different relationship between ENSO and the two interannual modes, the lead-lag correlation between PCs and ENSO indices is shown in Figure 7. EEM in NCEP data is negatively correlated with ENSO index simultaneously and in the subsequent ten months (Figure 7(a), solid

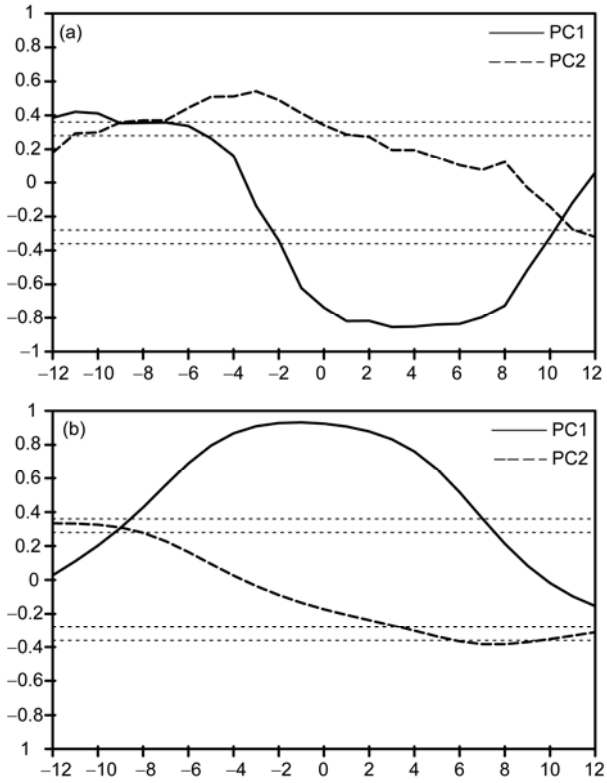

Figure 7 (a) Lead-lag correlation between PC1 and Niño3.4 index (solid line), and between PC2 and Niño3.4 index (dashed line) for NCEP data, where abscissa represents the number of months Niño3.4 index lagging JJA. (b) Same as in (a) but for model results. Horizontal dotted lines in each panel represent the 95% and 99% confidence level.

line), indicating that the EEM tends to accompany La Niña condition in the subsequent ten months. EWM in NCEP data is positively correlated with ENSO index in the subsequent several months but cannot exceed the confidence level (Figure 7(a), dashed line), indicating it is not a precursor of ENSO evolution. The relationship between EEM and ENSO phase transition is not evident in the simulation. Although the quasi-two year period of EEM is clear in FGOALS_gl (Figure 2(d)), the simulated period of ENSO is longer than the observation [24]. Therefore, the excessively long ENSO period in the simulation is probably due to the failure in simulating the influence of the NWPAC on ENSO phase transition. On the other hand, the simulated EWM is highly positively correlated with ENSO in the antecedent and subsequent half year, again implying that the simulated EWM is dominated by ENSO.

The regressed vertical velocity at 500 hPa and velocity potential at 200 hPa are examined in Figure 8 to check how convection and Walker circulation response to SSTA. Associated with EEM, both NCEP and FGOALS_gl show enhanced Pacific Walker circulation, with upper troposphere convergence, middle troposphere descent, and lower troposphere divergence over central-eastern Pacific, and the opposite over the maritime continent (Figure 8(a), (b), (g), (h)). The main deficiency of the model is that the simulated divergent circulation is rather weak and not statistically significant at the 5% level in many regions (Figure 8(h)). The EWM in both NCEP and FGOALS_gl is associated with a weakened Pacific Walker circulation (Figure 8(c)–(f)). The main difference between reanalysis and simulation is seen over the Indian Ocean. Convergence over the Indian Ocean at 200 hPa is seen in the simulation but not in NCEP data. This bias is probably due to excessively westward extension of warm SSTA with Walker circulation anomaly over the Pacific in the model.

The above analysis shows that there are distinct mechanisms for the distinct modes, related to different ENSO condition. The SSTA pattern over the tropical Pacific associated with the two modes in this study is consistent with Chung et al. [9], which was derived by decomposing NWPAC index into 2–3-year and 3–5-year components and regressing SSTA onto these components. Although most recent research emphasizes the contribution of the Indian Ocean, this work suggests that the tropical Pacific Ocean is more important for the interannual variability of the NWPAC. The results from FGOALS_gl simulation are more consistent with the reanalysis over the Pacific than that over the Indian Ocean. The role of the Indian Ocean deserves further study.

5 Summary and discussion

5.1 Summary

Two distinct modes of the interannual variability of the NWPAC are revealed by using NCEP reanalysis data and the output of 20C3M simulation by FGOALS_gl. Dependent on the associated anomalous equatorial zonal wind, these two modes are termed as “Equatorial Easterly related Mode” (EEM) and “Equatorial Westerly related Mode” (EWM), respectively. We found that although the formation mechanisms of these two modes are similar, the maintenance mechanisms, dominant periods, and the relationships with ENSO differ. The major findings are summarized below:

(1) The interannual variability of the NWPAC represented by 850 hPa wind exhibits two dominant periods: quasi-two years (2–3 years) and quasi-five years. Both of them are evident in the NCEP reanalysis data and the simulation. The two distinct modes of the interannual variability of the NWPAC are identified by performing multivariate EOF analysis on 850 hPa wind. They are termed as “Equatorial Easterly related Mode” (EEM) and “Equatorial Westerly related Mode” (EWM) in terms of the anomalous zonal wind along the equator, respectively. These two modes have a similar formation mechanism, but differ in their maintenance mechanism, dominant period and the relationship with ENSO condition.

(2) The first two leading modes are both featured by an anomalous NWPAC. The anomalous NWPAC forms in the

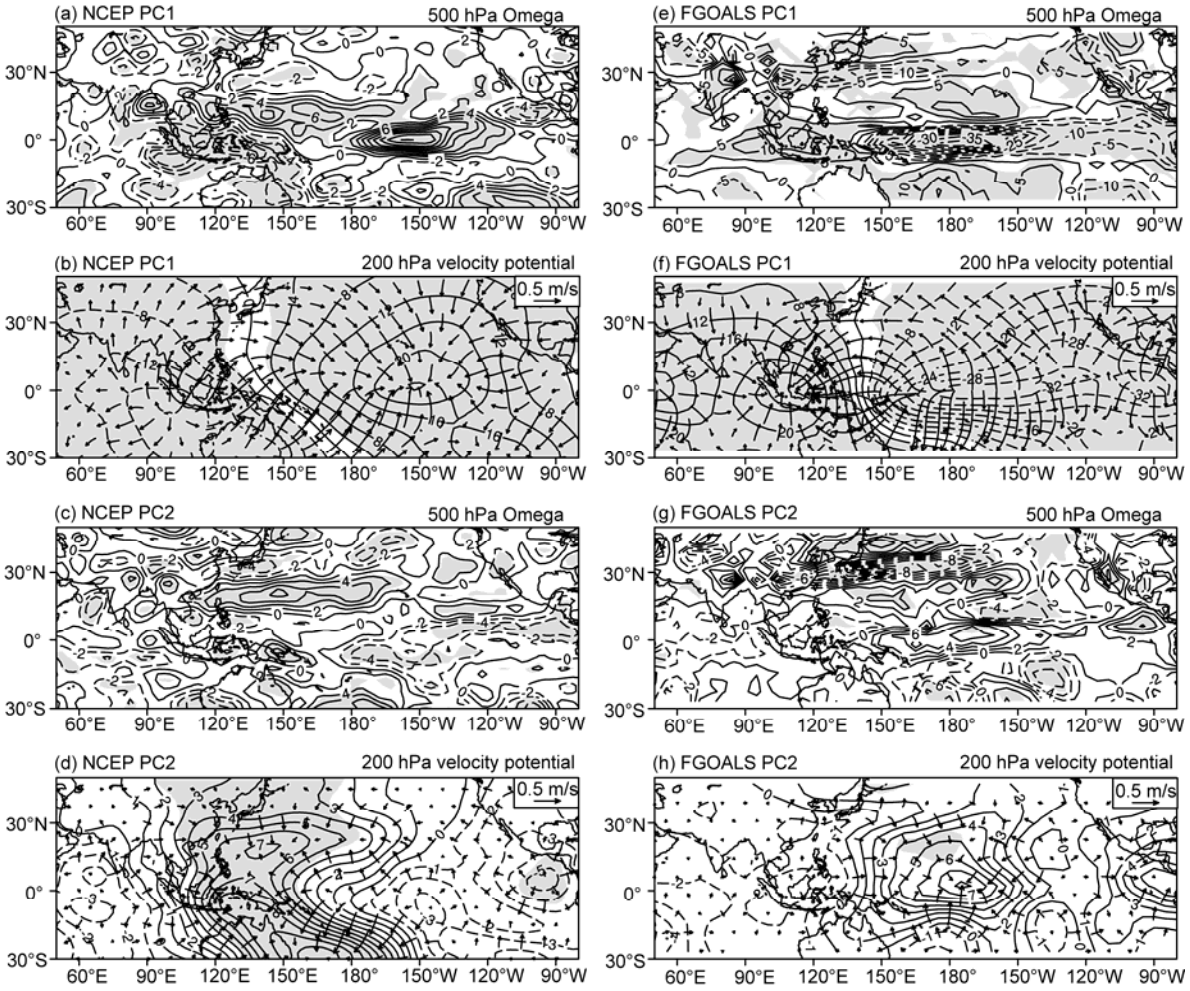

Figure 8 (a) 500 hPa vertical velocity (unit: Pa/s, negative value represents ascent) regressed onto NCEP PC1. (b) 200 hPa velocity potential regressed onto NCEP PC1, where divergent wind is represented as arrows. (c) and (d) are the same as in (a) and (b), but for NCEP PC2. (e)–(h) are identical to (a)–(d) except for model result. Regions exceeding 95% confidence level are shown as gray shading in each panel.

preceding winter-half year when the low-latitude of the northern hemisphere is controlled by northeasterly trade wind. Warm SSTA in the equatorial central-eastern Pacific induces local ascent motion, heating the atmosphere and leading to cyclonic Rossby wave response along the dateline. The anomalous northeasterly on the western flank of this anomalous cyclonic circulation induces a cold SSTA belt over the central Pacific by enhancing evaporation. The anomalous NWPAC is triggered by the negative heat source over the central Pacific associated with the cold SSTA.

(3) EEM is accompanied by El Niño decaying and transition to La Niña. The anomalous NWPAC has been established in the previous fall or winter trigged by El Niño condition. Although warm SSTA over the central-eastern Pacific has vanished in spring and been transformed to cold phase in summer, the anomalous NWPAC persists into summer maintained by local air-sea interaction. Anomalous equatorial upwelling, induced by the anomalous easterly on the southern flank of the anomalous NWPAC, favors the development of La Niña. This interaction between EEM and ENSO contributes to the quasi-two year oscillation of the NWPAC-ENSO system.

(4) EWM is associated with persisting El Niño since the previous fall. The anomalous NWPAC is formed in spring and maintained by remote forcing from the central-eastern Pacific. As warm SSTA in the central-eastern Pacific persists through the whole summer, the anomalous NWPAC gets strengthened in summer.

(5) These two interannual modes of the NWPAC are well reproduced by FGOALS_gl in terms of spatial pattern, but not their relative importance. EEM (EWM) is the first (second) mode in NCEP reanalysis data, accounting for 35.6% (19.3%) of the total variance. However, in FGOALS_gl, EWM (EEM) becomes the first (second) mode, accounting for 66.2% (10.7%) of the total variance. Excessively strong EWM in FGOALS_gl is probably due to the bias in the peaking season and period of ENSO. The simulated ENSO generally peaks in spring or summer, leading to overly strong forcing on the summer NWPAC. The dominant period of simulated ENSO is quasi-five year, inducing exces-

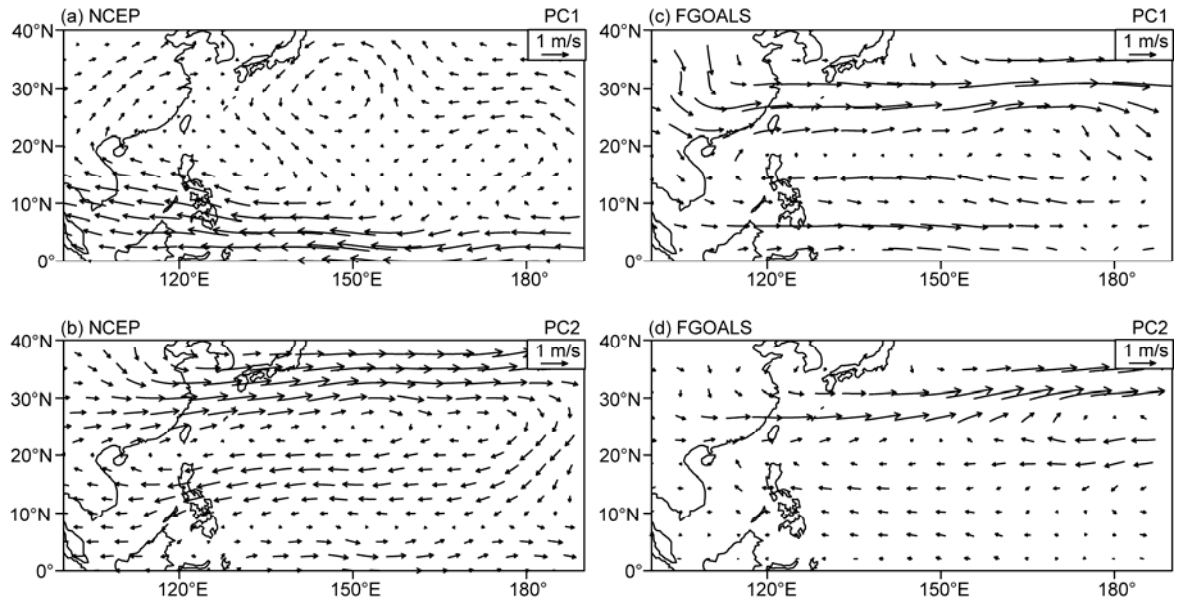

Figure 9 500 hPa wind field in the concurrent summer regressed onto NCEP PC1 (a) and NCEP PC2 (b). (c) and (d) are the same as in (a) and (b) but for model result.

sively strong quasi-five year oscillation of the NWPAC in the model. Insufficient EEM in FGOALS_gl is associated with the absence of the influence of the anomalous NWPAC on tropical oceans. The SSTA reversal from warm to cold condition over the central-eastern Pacific is not reproduced by FGOALS_gl, leading to weaker quasi-two year oscillation of the monsoon-ENSO system.

5.2 Discussion

Traditional investigation on the relationship between the NWPAC and East Asian climate focuses on circulation at 500 hPa. Since recent research on subtropical anticyclone and the associated air-sea interaction pays more attention to the lower troposphere, such as sea level pressure and wind at 850 hPa, this work focuses instead on 850 hPa. What are the circulation anomalies at 500 hPa associated with the two interannual modes that are derived from wind field at 850 hPa? Figure 9 shows the corresponding anomalous wind at 500 hPa by regressing the wind components onto the PCs shown in Figures 3 and 4. The anomalous winds at 500 hPa (Figure 9(a), (b)) in the NCEP reanalysis are similar to those of 850 hPa (Figure 3(a), (d)). Both of them show anomalous anticyclones to the north of the Philippines (over the NWP within 10°–30°N) and anomalous easterly (westerly) along the equator in EEM (EWM). Compared with climatological wind at 500 hPa (Figure 1(d)), EWM indicates an intensification of subtropical high at 500 hPa. In the model, the wind anomalies at 500 hPa (Figure 9(c), (d)) also show high consistency with that at 850 hPa (Figure 4(a), (d)), with the anomalously strong NWPAC at 500 hPa. Therefore, our result is insensitive to the vertical levels.

The relative importance of the two modes is not reasonably captured by the model, which is attributed partly to the bias of the model in ENSO simulation. However, some other possible causes should not be excluded, such as the NWP local heating [17], anomalous convection in warm pool region [39], the upper troposphere dynamics [40], and the forcing from the Indian Ocean [15, 16]. The aim of this paper is to reveal the characteristic and mechanism of the interannual variation of the NWPAC and to evaluate their performance in FGOALS_gl. To understand the reason of model bias, a series of sensitivity experiments are required in future study.

The authors are grateful to the two anonymous reviewers for their useful comments and suggestions. This work was supported by National Natural Science Foundation of China (Grant Nos. 40890054 and 41125017).

1 Tao S Y, Chen L X. A review of recent research on East Asian summer monsoon in China. In: Chang C P, Krishnamurti T N, eds. Monsoon Meteorology. London: Oxford University Press, 1987. 60–92
2 Zhou T J, Yu R C. Atmospheric water vapor transport associated with typical anomalous summer rainfall patterns in China. J Geophys Res, 2005, 110: D08104
3 Zhang Q Y, Tao S Y, Chen L T. The inter-annual variability of East Asian summer monsoon indices and its association with the pattern of general circulation over East Asia (in Chinese). Acta Meteor Sin, 2003, 61: 559–568
4 Chang C P, Zhang Y S, Li T. Interannual and interdecadal variations of the East Asian summer monsoon and tropical Pacific SSTs. Part I: Roles of the subtropical ridge. J Clim, 2000, 13: 4310–4325
5 Lu R Y. Indices of the summertime western North Pacific subtropical high. Adv Atmos Sci, 2002, 19: 1004–1028
6 Wu G X, Liu Y M, Liu P. The effect of spatially nonuniform heating on the formation and variation of subtropical high I: Scale analysis (in Chinese). Acta Meteor Sin, 1999, 57: 257–263
7 Liu Y M, Wu G X, Ren R C. Relationship between the subtropical anticyclone and diabatic heating. J Clim, 2004, 17: 682–698

8 Lu R Y. Interannual variability of the summertime North Pacific subtropical high and its relation to atmospheric convection over the warm pool. J Meteor Soc Jpn, 2001, 79: 771–783
9 Chung P H, Sui C H, Li T. Interannual relationships between the tropical sea surface temperature and summertime subtropical anticyclone over the western North Pacific. J Geophys Res, 2011, 116: D13111
10 Wu B, Zhou T J. Oceanic origin of the interannual and interdecadal variability of the summertime western Pacific subtropical high. Geophys Res Lett, 2008, 35: L13701
11 Lu R Y, Fu Y H. Summer climate variability in East Asia and the western North Pacific and its mechanisms (in Chinese). Adv Earth Sci, 2009, 24: 123–131
12 Yang H, Sun S Q. Longitudinal displacement of the subtropical high in the western Pacific in summer and its influence. Adv Atmos Sci, 2003, 20: 921–933
13 Lu R Y, Li Y, Ryu C S. Relationship between the zonal displacement of the western Pacific subtropical high and the dominant modes of low-tropospheric circulation in summer (in Chinese). Prog Nat Sci, 2007, 17: 546–550
14 Wang B, Wu R G, Fu X H. Pacific-East Asian teleconnection: how does ENSO affect East Asian climate? J Clim, 2000, 13: 1517–1536
15 Xie S P, Hu K M, Hafner J, et al. Indian Ocean capacitor effect on Indo-Western Pacific climate during the summer following El Niño. J Clim, 2009, 22: 730–747
16 Wu B, Zhou T J, Li T. Seasonally evolving dominant interannual variability modes of East Asian climate. J Clim, 2009, 22: 2992–3005
17 Wu B, Li T, Zhou T J. Relative contributions of the Indian Ocean and local SST anomalies to the maintenance of the Western North Pacific anomalous anticyclone during the El Niño decaying summer. J Clim, 2010, 23: 2974–2986
18 Li Y, Yang X Q, Xie Q. Selective interaction between interannual variability of North Pacific Subtropical High and ENSO cycle (in Chinese). Chin J Geophys, 2010, 53: 1543–1553
19 Kug J S, Kang I S. Interactive feedback between ENSO and the Indian Ocean. J Clim, 2006, 19: 1784–1801
20 Park J Y, Jhun J G, Yim S Y, et al. Decadal changes in two types of the western North Pacific subtropical high in boreal summer associated with Asian summer monsoon/El Niño-Southern Oscillation connections. J Geophys Res, 2010, 115: D21129
21 Zhou T J, Yu Y Q, Liu H, et al. Progress in the development and application of climate ocean models and ocean-atmosphere coupled models in China. Adv Atmos Sci, 2007, 24: 1109–1120
22 Yu Y Q, Zhi H, Wang B, et al. Coupled model simulations of climate changes in the 20th century and beyond. Adv Atmos Sci, 2008, 25: 641–654
23 Li B, Zhou T J, Wu C Q, et al. Relationship between rainfall and sea surface temperature simulated by LASG/IAP AGCM and CGCM (in Chinese). Chin J Atmos Sci, 2009, 33: 1071–1086
24 Man W M, Zhou T J, Zhang L X. The tropical Pacific interannual variability simulated with LASG/IAP climate system model (in Chinese). Chin J Atmos Sci, 2010, 34: 1141–1154
25 Zhou T J, Li B, Man W M, et al. A comparison of the Medieval Warm Period, Little Ice Age and 20th century warming simulated by the FGOALS Climate System Model. Chin Sci Bull, 2011, 56: 3028–3041
26 Man W M, Zhou T J. ForcedrResponse of atmospheric oscillations during the Last Millennium simulated by a Climate System Model. Chin Sci Bull, 2011, 56: 3042–3052
27 Kalnay E, Kanamitsu M, Kistler R, et al. The NCEP/NCAR 40-year reanalysis project. Bull Amer Meteorol Soc, 1996, 77: 437–471
28 Smith T M, Reynolds R W. Improved extended reconstruction of SST (1854–1997). J Clim, 2004, 17: 2466–2477
29 Zhou T J, Wu B, Wen X Y, et al. A fast version of LASG/IAP climate system model and its 1000-year control integration. Adv Atmos Sci, 2008, 25: 655–672
30 Zhou T J, Yu R C. Twentieth century surface air temperature over China and the globe simulated by coupled climate models. J Clim, 2006, 19: 5843–5858
31 Man W M, Zhou T J, Zhang J, et al. The temperature evolution during the 20th century as simulated by the climate system model FGOALS-gl (in Chinese). Acta Meteorol Sin, 2011, 69: 644–654
32 Huang G, Hu K M, Xie S P. Strengthening of tropical Indian Ocean teleconnection to the Northwest Pacific since the mid-1970s: An atmospheric GCM study. J Clim, 2010, 23: 5294–5304
33 Li W H, Li L F, Fu R, et al. Changes to the North Atlantic subtropical high and its role in the intensification of summer rainfall variability in the Southeastern United States. J Clim, 2011, 24: 1499–1506
34 Zhou T J, Yu R C, Zhang J, et al. Why the Western Pacific Subtropical High has extended westward since the late 1970s. J Clim, 2009, 22: 2199–2215
35 Mu Q Z, Wang S W, Zhu J H, et al. Variations of the Western Pacific Subtropical High in summer during the last hundred years (in Chinese). Chin J Atmos Sci, 2001, 25: 787–797
36 Zhao Z G. Summer Drought and Flood over China and the Environmental Field (in Chinese). Beijing: China Meteorological Press, 1999. 45–52
37 Wang B. The Vertical structure and development of the ENSO anomaly mode during 1979–1989. J Atmos Sci, 1992, 49: 698–712
38 Gill A E. Some simple solutions for heat-induced tropical circulation. Quart J Roy Meteor Soc, 1980, 106: 447–462
39 Lu R Y, Dong B W. Westward extension of North Pacific subtropical high in summer. J Meteor Soc Jpn, 2001, 79: 1229–1241
40 Enomoto T. Interannual variability of the Bonin high associated with the propagation of rossby waves along the Asian jet. J Meteor Soc Jpn, 2004, 82: 1019–1034